Journal of
Materials Chemistry B

Materials for biology and medicine

Accepted Manuscript

This article can be cited before page numbers have been issued, to do this please use: T. Zhang, Z. Liu, H. Aslan, C. Zhang and M. Yu, *J. Mater. Chem. B*, 2020, DOI: 10.1039/D0TB00935K.

ROYAL SOCIETY OF CHEMISTRY

rsc.li/materials-b

View Article Online
DOI: 10.1039/D0TB00935K

ARTICLE

NIR-Responsive Reversible Phase Transition of Supramolecular Hydrogels for Tumor Treatment

Received 00th January 20xx,
Accepted 00th January 20xx

DOI: 10.1039/x0xx00000x

Ting Zhang,[a] Zhiyu Liu,[c] Hüsnü Aslan,[d] Chunhua Zhang*[a] and Miao Yu*[b]

Locally administrable drugs with controllable release on external cue holds great promise for antitumor therapy. Here, we report an injectable, supramolecular hydrogel (SHG), where the drug release can be controllably driven by near infrared (NIR) irradiation. The SHGs are formed by electrostatic interaction with laponite (XLG), in which upconverting nanoparticles (UCNPs) modified with α-cyclodextrin (α-CD) are used as the core, and azobenzene quaternary ammonium salt (*E*-azo) are further assembled through host-guest interaction. The hydrogel demonstrates reversible phase transition between gel and sol state and photothermal conversion capability. In detailed *in vitro* and *vivo* trials, drug-loaded SHGs successfully suppressed invasion by cancer cells. Such phase transition by remote NIR-switch hence the photothermal effect-promoted drug release emphasizes the considerable potential of supramolecular hydrogel in anticancer therapies, espeically for the treatments requiring long-term, on-demand drug supply in clinic.

Introduction

Designing and synthesizing nano-assemblies by supramolecular chemistry for tumor therapy have become a fascinating strategy.[1] Besides the distinct merits, such as predictability, reversibility, and adjustability, supramolecular assemblies (*e.g.* micelles, vesicles, hydrogels, *etc.*) have sensitive response to various triggers.[2] Small shifts in environmental pH, temperature, light, ionic strength or solvent polarity are often adequate to induce dramatic changes of their assembly form,[3] showing promising potential for controlled delivery of drugs and genes.[4]

Supramolecular hydrogels (SHGs), which are combined by reversible non covalent interactions among their constituent molecules including hydrogen bonding, electrostatic interaction, metal ligand coordination and hydrophobic association, have attracted much interest as biomaterials, binder, sewage treatment and 4D printing.[5] Compared to fully covalent crosslinked hydrogels, they are opaque, fragile and irreparable, SHGs could be customized in biomedical applications to match the mechanical properties and properties of target biological tissues, such as on-demand reversible gel behavior, self-healing ability, thixotropy and stimulation reactivity.[6] As drug carriers, SHGs present good biocompatibility and degradability, efficient drug loading and appropriate protection on labile drugs from degradation, together with spatial/temporal control of the drug release.[7] To avoid invasive implantation and risks associated with surgery, injectable SHGs, especially their on-demand drug release at the tumor site driven by external light, have sparked considerable interest.[8] However, most of the developed SHGs drug carriers were ultraviolet (UV)/visible light-responsive, which are undesirable due to the limited penetration and irradiation damage.[9] In this regard, near infrared (NIR) light-activated drug release of SHGs is highly preferred.[10]

Herein, we report an injectable SHG as a high-load drug carrier, where the drug release is driven by NIR irradiation. As illustrated in **Scheme 1**, upconverting nanoparticles (UCNPs), *i.e.* $NaYF_4$:Yb^{3+},Tm^{3+}@$NaYF_4$, are fabricated as the core and covalently coated by α-cyclodextrin (α-CD), which are further assembled with azobenzene quaternary ammonium salt (*E*-azo) through host-guest interaction. The resultant UCNP@α-CD-*E*-azo forms a stable, injectable SHG with laponite (XLG) clay *via* electrostatic interaction, showing high biocompatibility and stability. Upon NIR irradiation, the UCNPs convert the absorbed NIR light into UV emission and heat, inducing *E*-to-*Z* isomerization of azo hence a gel-to-sol phase transition, which is promoted by the photothermal effect. The phase transition then enables the drug release efficiently. As the phase transition is reversible, the drug release can be turned in a controlled manner by switching the irradiation. Such a high-

[a] T. Zhang, Prof. C. H. Zhang, MIIT Key Laboratory of Critical Materials Technology for New Energy Conversion and Storage, School of Chemistry and Chemical Engineering, Harbin Institute of Technology, P. O. Box 1254, Harbin, 150001, P. R. China. Email: zhangchunhua@hit.edu.cn
[b] Prof. M. Yu, School of Chemistry and Chemical Engineering, Harbin Institute of Technology, Harbin, 150001, P. R. China. Email: miaoyu_che@hit.edu.cn
[c] Z. Liu, Department of Chemistry and Biochemistry, University of California, Los Angeles, Los Angeles, California 90095
[d] Dr. A. Hüsnü, Interdisciplinary Nanoscience Center (iNANO), Aarhus University, The iNANO House, Gustav Wieds Vej 14, 8000 Aarhus C
† Footnotes relating to the title and/or authors should appear here.
Electronic Supplementary Information (ESI) available: [details of any supplementary information available should be included here]. See DOI: 10.1039/x0xx00000x

View Article Online
DOI: 10.1039/D0TB00975K

load, biocompatible drug carrier with switchable, controllable drug release upon NIR holds great promise for antitumor treatments in clinic.

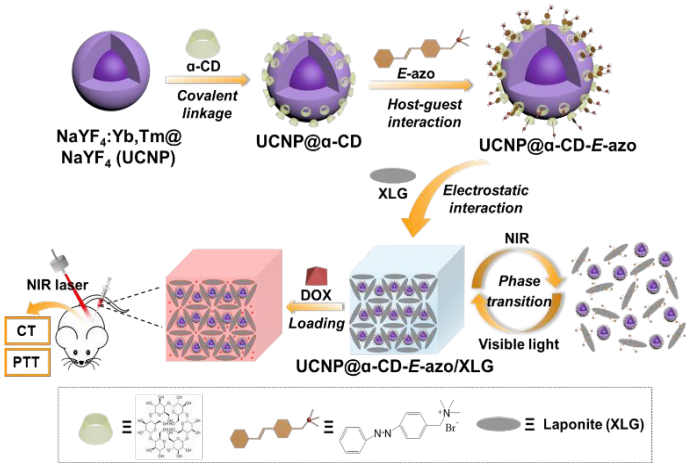

Scheme 1 Schematic illustration of the assembly and NIR-triggered phase transition of the injectable SHGs.

Experimental section

Characterization. ^{1}H NMR, ^{13}C NMR spectra and NOESY spectrum were measured by a Bruker AVANCE AV400. ESI-MS were recorded on a Agilent 6520 Q-TOF-MS. TEM images and SEM images were examined by a Philips EM400st transmission electron microscope and a JEOL JSM-7500F scanning electronic microscope, respectively. UV/vis spectra were recorded on a Shimadzu UV-3600 spectrophotometer equipped with a PTC-348 WI temperature controller. X-ray diffraction (XRD) was conducted using a Siemens D5005 diffractometer with Cu Kα radiation at 40 kV and 30 mA. Zeta potential and the dynamic light scattering (DLS) were measured by Brookhaven Instruments at 25 °C. Rheological tests of hydrogels were carried out by using an Anton Paar model MCR-301 rheometer, with a 25 mm diameter parallel plate attached to a transducer. Thermal gravimetric analysis (TGA) were measured by using a NETZSCH TG209 under N_2 atmosphere. The fluorescence spectra were surveyed by HORIBA FL-3. NIR laser light (980 nm) source come from Hi-tech optoelectronics Co.,Ltd.

Materials. Unless otherwise specified, all solvents and reagents could be used directly without further treatment. Rare earth compounds ($YCl_3{\cdot}6H_2O$, $YbCl_3{\cdot}6H_2O$, $TmCl_3{\cdot}6H_2O$), N, N-diisopropylethylamine, oleic acid, 1H-benzotriazol-1-yloxytripyrrolidinophosphonium hexafluorophosphate are all obtained from Aladdin. And 1-octadecene, 3-(4,5-Dimethylthiazol-2-yl)-2,5-diphenyltetrazolium bromide (MTT), propidiumiodide (PI) and 4,6-diamidino-2-phenylindole (DAPI) are purchased from Sigma-Aldrich. Glyphosine (Gly) is purchased from Macklin. Laponite (XLG) is bought from Rockwood Additives Ltd.

Synthesis of UCNP-Gly. Approximately 150 mg of precipitated UCNPs were added to a 50.0 mL flask along with 8.0 mL $CHCl_3$ and absolute 2.0 mL EtOH. Then, 600.0 mg glyphosine (Gly) were added to the mixture of 2.0 mL $CHCl_3$ and absolute 2.0 mL EtOH. The mixture solution were stirred overnight with vigorous magneticly at room temperature, at which point it was transferred to a centrifuge tube and then hexanes were added. The UCNP-Gly were collected by centrifugation at 8000 rpm for 15 min and dried in a vacuum.

Synthesis of UCNP@α-CD. α-CD-NH-NH_2 was prepared according to previous reference.[11] The precipitated 50 mg UCNP-Gly nanoparticles were redispersed in anhydrous DMF (3.0 mL). And α-CD-NH-NH_2 (300 mg), N, N-diisopropylethylamine (82.5 mg), 1H-benzotriazol-1-yloxytripyrrolidinophosphonium hexafluorophosphate (132.8 mg) were added into the solution. The solution was intensely stirred two days under N_2 atmosphere and centrifuged. The as-prepared nanoparticles were dispersed in distilled water, and excess ligands and catalysts were removed through dialysis.

Synthesis of compound (*E*)-*N*,*N*,*N*-trimethyl-1-(4-(phenyldiazenyl)phenyl)methanaminium (*E*-azo). Firstly, the mixture of 2.70 g p-aminotoluene, 2.70 g nitrosobenzene and 30.0 mL acetic acid were added to a round bottom flask and stirred for 24 h vigorously under N_2 atmosphere. The precipitate were separated by column chromatography to afford a red solid compound **1** (55%). Then, 1.0 g as-prepared compound **1**, 1.1 g N-bromosuccinimide (NBS) and 65.0 mg α-azoisobutyronitrile (AIBN) were added to 20.0 mL CCl_4 and refluxed for 24 h. The product were collected through vacuum distillation and purificated by column chromatography on silica gel to get the red solid compound **2** (82.0%). When *E*-azo was synthesized, a solution of 2.70 g compound **2** in 25.0 mL ethanol and 25.0 mL trimethylamine (30.0% in ethanol) were reacted at 80 °C for 24 h. The solution was concentrated by decompression, further dissolved in water and washed several times with dichloromethane. The crude product was further crystallized and purified by methanol, and dried in vacuum at 50℃ to obtain the pure orange-yellow solid (50.0%). ^{1}H NMR (400 MHz, D_2O) δppm = 7.85 (d, 2H), 7.80 (d, 2H), 7.66 (d, 2H), 7.54 (m, 3H), 4.48 (s, 2H), 3.05 (d, 9H). ^{13}C NMR (400 MHz, D_2O) δppm =153.33, 152.03, 133.99, 132.26, 130.16, 122.74, 68.84, 52.45. HRMS [M-Br]$^-$ calcd for $C_{16}H_{20}N_3^+$: 254.1652. Found: 254.1655.

Synthesis of supramolecular hydrogels (SHGs). 100.0 mg Laponite (XLG) were suspensed in 4.0 mL deionized water with vigorously stirring for 15 min at 25 °C. Then, 3.0 mg, 0.5 mL sodium polyacrylate was added into the solution and reacting for 20 min. Nextly, a solution of UCNP@α-CD-*E*-azo (38.5 mg, 0.5 mL) was added and kept stirring for 3 min. After the reaction, the SHGs remained upright and stationary for 1 h.

Drug loading and releasing in *vitro*. In the process of DOX-loaded supramolecular hydrogel synthesis, 100.0 mg XLG were suspensed in 4.0 mL deionized water with vigorously stirring for 15 min at 25 °C. Then, 3.0 mg, 0.5 mL sodium polyacrylate was added into the solution and reacting for 20 min. Nextly, a solution of UCNP@α-CD-*E*-azo (38.5 mg, 0.5 mL) and 5 mg DOX were simultaneously added and mixed to prepare DOX-UCNP@α-CD-*E*-azo/XLG. The calculation formula of DOX encapsulation rate was as follows:

$$\text{DOX encapsulation rate (\%)} = (m_L/m_0) \times 100\ \%$$

where m_L and m_0 are mass of DOX loaded in the UCNP@α-CD-*E*-azo/XLG supramolecular hydrogel and mass of DOX added,

respectively. The mass of DOX was determined at 480 nm by a UV spectrophotometer. 5.0 mg DOX-UCNP@α-CD-*E*-azo/XLG supramolecular hydrogel were fully dissolved in 15.0 mL PBS of different pH values under conditions of darkness or 980 nm (1 W cm^{-2}, 2 W cm^{-2}, 3 W cm^{-2}) laser illuminate for different time. At different points in time, the samples were centrifuged, and the supernatant was examined by UV-Vis spectroscopy to determine the dose released.

In *vitro* cell cytotoxicity assay. The MTT assay on HepG2 (hepatoma cell line) cells and L02 (normal human liver cells) cells were used to analyze the cell viability in *vitro*. HepG2 cells and L02 cells were seeded into 96-well plates for 24 h with a density of 1.0×10^4 per well in 100 μL DMEM medium, respectively. Then, different concentrations of UCNP@α-CD-*E*-azo/XLG and DOX-UCNP@α-CD-*E*-azo/XLG were added and continued to incubate for 24 h. Nextly, 20.0 μL, 5.0 mg mL^{-1} MTT solution was added into per well and incubated for another 4 h. After that, the media was removed and 150.0 μL DMSO was added for 0.5 h then replaced and wanshed. Finally, the absorbance was monitored at 490 nm by a microplate reader (SynergyTM HT).

Fluorescence imaging. For observing cellular uptaking and DOX releasing, HepG2 cells were incubated in a 6-well plates for 24 h. Then, UCNP@α-CD-*E*-azo/XLG and DOX-UCNP@α-CD-*E*-azo/XLG were added into the above medium for 6 h at a dose of 250.0 μg mL^{-1}. Then washing medium three times with PBS, the cleaned medium were added into the culture plate. And the medium were exposed with NIR light (980 nm, 1.0 W cm^{-2}) for 30 min. After incubation, PI was added and stained for 30 min, then washed with PBS for several times. Similarly, in the cell uptake experiment, DAPI was added to the culture medium and dyed for 30 min. Finally, the medium were washed with PBS for three times and exposed with NIR light (980 nm, 1.0 W cm^{-2}) for 30 min. The fluorescence images were observed in a Leica DFC450 C Microsystems.

Confocal laser scanning microscopy (CLSM). Firstly, 5.0×10^4 HepG2 cells were cultured in 0.5 mL DMEM for 24 h in coverglass bottom dishes of 6-well plates at 37 °C. After incubating with DOX-UCNP@α-CD-*E*-azo/XLG for 6 h, the culture medium was discarded. Then, the medium washed with PBS three times and exposed with NIR light (980 nm, 1.0 W cm^{-2}) for different time. Nextly, DAPI was added into the medium and followed by incubation for 15 min. The medium was washed with PBS for several times, and 1 mL PBS solution were added. The CLSM images were acquired using Confocal Software (FluoView FV1000, Olympus).

In *vivo* antitumor effect. For animal experiments, female Balb/c nude mice which about four or five weeks old were bought from Vital River Laboratory Animal Technology Co., Ltd. And all animal were implemented in accordance with the standard of the National Regulation of China for Care and Use of Laboratory Animals. Then, HepG2 cells were distributed in DMEM to build tumor models, and followed by injecting Matrigel in the left front leg of all mice. Untill tumor volume grew to150 mm^3, all mice were divided in six groups randomly, five mice in each group. Group 1 (PBS solution), group 2 (NIR light irradiation), group 3 (UCNP@α-CD-*E*-azo/XLG), group 4 (UCNP@α-CD-*E*-azo/XLG with NIR light irradiation), group 5 (DOX-UCNP@α-CD-*E*-azo/XLG), and group 6 (DOX-UCNP@α-CD-*E*-azo/XLG with NIR light irradiation). Mice in the group were injected with 100 μL PBS or 100 μL, 1 mg mL^{-1} UCNP@α-CD-*E*-azo/XLG (UCNP@α-CD-*E*-azo:XLG=38.5:100 wt%) and DOX-UCNP@α-CD-*E*-azo/XLG (UCNP@α-CD-*E*-azo:XLG:DOX=38.5:100:5 wt%) intratumorally, respectively. After 2 h postinjection, the mice were exposured by NIR light (980 nm, 1.0 W cm^{-2}) for 30 min. After six groups of treatment, tumor volumes and weights of all mice were monitored daily and then normalized with the original values. The calculation equations of tumor volume (T_{volume}) was as follows:

$$T_{volume} = (T_{length}) \times (T_{width})^2/2$$

where T_{length} and T_{width} are length and width of tumor measured with a caliper, respectively. Relative T_{volume} was calculated for V/V_i, and relative T_{weight} were calculated for W/W_i. V_i and W_i are original values of mice.

Histology analysis. After treatment, the tumor sections and important organs (heart, spleen, liver, kidney and lung) of mice were collected, and fixed with 4% paraformaldehyde and embedded in paraffin. Staining with H&E was applied to the main organs and tumor sections of mice for histological analysis. At last, Olympus BX53 fluorescence microscope was applied to obtain the optical microscope images.

Haematological analysis. Collecting 20 μL blood of all mice after treatment at 14th day and using a HF-3800 blood analyzer for haematological analysis.

RESULTS AND DISCUSSION

Construction of NIR-responsive supramolecular hydrogels (SHGs). The synthesis and characterization of compound *E*-azo are presented in the **Schemes S1** and **Fig. S1–S3**.[12] The oleic acid (OA)-capped UCNPs were produced according to the method reported previously.[13] Their transmission electron microscope (TEM) images showed monodisperse, uniform particles with an average size of ~30 nm (**Fig. S4a** and **S4b**). High-resolution TEM (HRTEM) images was shown in **Fig. S4a** inset, and X-ray diffraction pattern was displayed in **Fig. S5**, they revealed that the nanoparticles possess high crystallinity, where the d_{100} = 0.51 nm is well indexed to hexagonal $NaYF_4$. Next, OA on UCNPs was substituted by glyphosine ligands.[14] The carboxylic group of the glyphosine ligands facilitated conjugation with ethanediamine-functionalized α-CD through a condensation reaction. The representative TEM, HRTEM, scanning electron microscope (SEM) images and XRD pattern of the obtained UCNP@α-CD (**Fig. S4c, S4d** and **S5**) indicated that the particles maintained similar size, morphology, and crystallinity like the UCNPs.

The covalent bonding of α-CDs on UCNPs was proved by the characterization of Fourier-transform infrared spectroscopy (FTIR). As shown in **Fig. S6**, compared with the strong bands at 2920 and 2850 cm^{-1} ascribed to the stretching vibration of CH_2 groups for UCNPs, additional bands at 1156 and 925 cm^{-1} (corresponding to the stretching vibration of P=O groups and P–OH groups, respectively), 1420 cm^{-1} (attributed to the typical symmetric stretching vibration of carboxyl), 3300 cm^{-1} (dued to

the stretching vibration of NH_2), 754 and 701 cm^{-1} (ascribed to the bending vibration of NH), and 1638 cm^{-1} (associated with the stretching vibrations of amide), appeared in the spectrum of UCNPs@α-CD, suggesting the presence of ethylenediamine-modified α-CD. Moreover, the evident change from being hydrophobic to hydrophilic (photos in **Fig. S7**) and the varied zeta potential (**Fig. S8**) from +17.69 ± 0.92 mV to –6.50 ± 0.34 mV also supported a successful surface modification by α-CD. Thermogravimetric analysis (TGA) showed that the α-CD-NH-NH_2 content in UCNP@α-CD was ~11.1% (**Fig. S9**).[15]

Photoluminescence (PL) spectra of UCNPs and UCNP@α-CD were collected with the excitation wavelength of 980 nm (**Fig. S10**), showing three emission peaks at ~360, 452 and 474 nm, which corresponded to the $^1D_2 \rightarrow {}^3H_6$, $^1D_2 \rightarrow {}^3F_4$, and $^1G_4 \rightarrow {}^3H_6$ transition from Tm^{3+}, repectively. And decreased emission intensity of UCNP@α-CD relative to that of UCNPs may be mainly dued to the light-scattering effect caused by modification of α-CD. Directly illustrated by the inset photo in **Fig. S10**, the significant PL emission also suggests the potential for imaging and sensing of the product.[16]

To further modify the particles using host-guest chemistry, we first investigated the interaction between α-CD and *E*-azo by ^1H nuclear magnetic resonance (NMR) titration method, indicating that these two components followed α-CD:*E*-azo=1:1 binding (**Fig. S11**). Following a nonlinear least squares curve-fitting method, the corresponding K_S value was calculated to be 4.89×10^5 M^{-1}, based on the sequential changes in chemical shifts (δ) of H_d at gradually increased concentrations of α-CD.[17] Mixing α-CD with *E*-azo solution resulted in the signals of the azo groups had a significant downfield shift, and at the same time the proton signals for H_c and H_d, *i.e* (adjacent protons of diazo group on the two benzene rings) got broadened (**Fig. S12b and S12c**). The cross-peaks of the proton signals between the azo groups and α-CD in the NOESY spectrum (1:1 equimolar mixture of α-CD-*E*-azo) was shown in **Fig. S13a**, further confirmed that *E*-azo unit as a guest integrated into the cavity of a-CD molecule. In addition, a decrease in relative intensity and a small hypsochromic shift of the main absorption band of the *E*-azo chromophore (at 319 nm corresponding to π–π* transition) were detected from the mixture (**Fig. S14**). Meanwhile, the n–π* transition also caused the descent and widening of the absorption peak at 428nm. Above changes can be attributed to the intermolecular interactions and polarity changes of the chromophore, indicating the formation of α-CD-*E*-azo complex, in consistent with the literature.[18] The zeta potential of UCNP@α-CD-*E*-azo further increased to 15.88 ± 0.48 mV, due to the participation of positively-charged azo group (**Fig. S8**).

The SHG was fabricated *via* a hierarchical self-assembly strategy. Sodium polyacrylate modified XLGs were used to improve the electronegativity of the XLGs surface and enhanced the mechanical property of hydrogels by electrostatic interaction.[19] A decrease in zeta potential from -14.32 ± 0.85 mV (pure XLG) to -29.41 ± 1.1 mV (XLG-Sodium polyacrylate) demonstrated a successful modification of sodium polyacrylate (**Fig. S8**). Distinct from the aqueous solution of XLG alone (2 wt%) showing no gelation (**Fig. 1a**), mixture of UCNP@α-CD-*E*-azo and XLG solution formed transparent, typical hydrogel, which was readily transformed into free-standing product (**Fig. 1b**). The gel presented three-dimensional scaffolding frameworks constructed by thin flakes, integrating the polymer with the dark particles (**Fig. 1c** and **1d**).

Remarkably, upon a short 980 nm light illumination (1 W cm^{-2}, 30 min), pronounced gel-to-sol phase transition occurred (**Fig. 1e**), allowing the product to be injected through a narrow syringe needle (**Fig. 1f**). Remarkably, the phase transition was reversible, *i.e.* upon exposed by 420 nm visible-light (1 W cm^{-2}) for 10 min, the sol was changed back to gel. Such gel-to-sol and sol-to-gel phase transition can be repeatedly triggered by applying NIR and visible light alternatively.

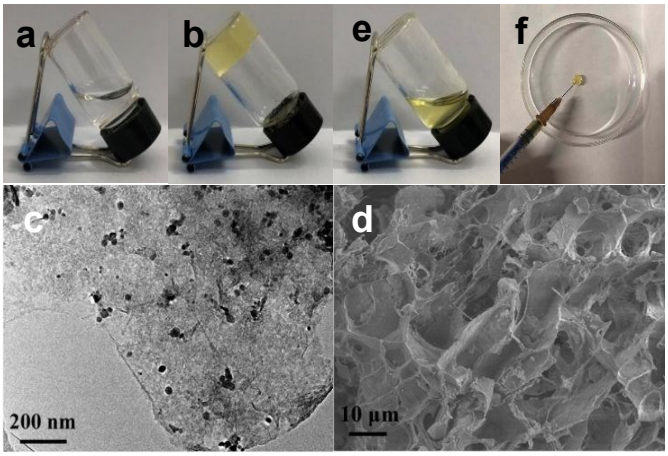

Fig. 1 Digital photos of (a) individual XLGs and (b) UCNP@α-CD-*E*-azo/XLG SHG, (c) TEM and (d) SEM images of UCNP@α-CD-*E*-azo/XLG SHG, (e) Photo of UCNP@α-CD-*E*-azo/XLG SHG under 980 nm irradiation (1 W cm^{-2}), (f) Demonstration of SHG injecting.

The phase transitionoriginates from the isomerism of *E*-azo. As shown in the ultraviolet-visible light (UV–vis) absorption spectra (**Fig. S15**), the absorbance of *E*-azo alone (0.05 mM) at 318 nm dropped to the lowest value upon UV irradiation (365 nm, 10 min), and restored upon visible light irradiation (420 nm, 40 s). The isomerization ratio of *E*-azo was estimated to be 67.87%. Consistently, the absorbance variation was reversible upon multiple repeated cycles of UV and visible light irradiation. Similar photo-induced isomerization also occurred in α-CD-*E*-azo, upon even shorter irradiation. UV irradiation as short as 3 minutes can already reduce the absorbance to the lowest value, and another visible light irradiation for just 20 s can restore the absorbance to the maximum (**Fig. S16**). The results suggest that the isomerization rate of *E*-azo can be improved by their integrating with macromolecular α-CD. The reversible photo-isomerization of α-CD-*E*-azo showed no obvious decay after multiple UV-visible light irradiation cycles.

In good accordance, after UV irradiation for 10 min, signals corresponding to the H_{c^*,d^*} protons in the ^1H NMR of α-CD-*E*-azo also showed significant up-field shift relative to $H_{c',d'}$ protons before irradiation (**Fig. S12c–d**). In comparison, the spectrum of *Z*-azo alone was barely varied under the same irradiation conditions (**Fig. S12a**). All these results suggested that the UV-

irradiation-induced *E*-to-*Z* isomerization of azo units can release the azo units from the a-CD cavity. The point was further confirmed by the vanished correlation peaks in the NOESY spectrum (**Fig. S13b**).

Similar *E*-to-*Z* isomerization occurred for the UCNP@α-CD-*E*-azo upon NIR irradiation with the isomerization rate in an irradiation power-dependent manner (**Fig. S17**), whilst no optical absorption variation were observed for α-CD-*E*-azo under the same conditions (**Fig. S18**). The results indicate that NIR-to-UV light conversion mediated by UCNPs can also induce the *E*-to-*Z* transformation of azo effectively in UCNP@α-CD-*E*-azo and lead to the gel-to-sol transition.

Mechanical properties of the SHGs. We then investigated mechanical properties of the SHGs by rheological experiments. When angular frequency of applied external strain was 0.1 rad s^{-1}, the storage moduli (*G′*) and loss moduli (*G″*) were plotted as functions (**Fig. 2a**). And *G′* and *G″* maintained practically constant and *G′* larger than that of *G″* at a strain from 0.1% to 10%. It demonstated that SHGs were steady and involved physical crosslinking were not compromised. When the strain is further increased, *G′* dropped faster than *G″* did. Under a strain of 50%, *G′* became smaller than *G″*, indicating the occurrence of gel-to-sol transition.

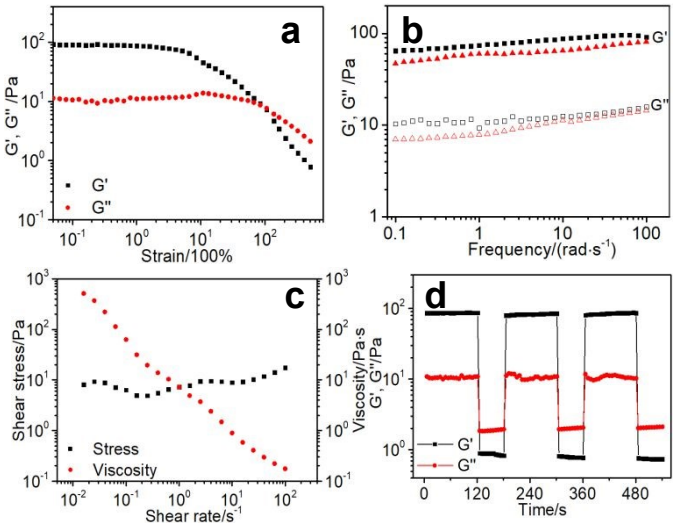

Fig. 2 (a) Dynamic strain scanning curves of the SHG when the angular frequency was 0.1 rad s^{-1}, (b) dynamic frequency scanning curves of the SHG (black squares) and after irradiation alternatively with NIR and visible light (red triangle) when the strain was of 1.0%, (c) the shear stress and viscosity of the SHG as the function of shear rate, and (d) the variations in strain amplitude of 100% and 0.1% alternatively for the SHG.

After analyzing the viscoelastic region, we chose strain of 1% to investigate the sensitivity of the gel to the oscillation frequency. As shown in **Fig. 2b** (black squares), *G′* was larger than *G″*, and both did not show any obvious change at an angular frequency from 0.1 to 100 rad s^{-1}, indicating gelation of product. Moreover, when the shear rate was 0.015 s^{-1} was applied, the viscosity of the SHGs reached the maximum, and produced the phenomenon of apparent decline as the shear rate further increased (**Fig. 2c**). We also evaluated the recovery performance of the gel by alternatively applying 100% and 0.1% strain amplitude, when the fixed frequency was 1.0 Hz. From **Fig. 2d**, SHGs exhibited liquid and solid state alternatively, showing swift response and reliable recovery. Besides, the rheological testing of the supramolecular hydrogels after alternating irradiation with NIR and visible light (Fig. 2b red triangle), showed no obvious mechanical strength loss as compared to the original hydrogel, thus indicating the complete recovery of the supramolecular hydrogel after the reversible light induced phase-transition process.

Drug Loading and Release Behaviors of the DOX-SHGs. To demonstrate drug loaded and delivery behaviors, doxorubicin (DOX), a typical chemotherapeutic drug, was selected as an example. DOX was mixed with UCNP@α-CD-*E*-azo and XLG to form the drug-loaded hydrogel, *i.e.* DOX/UCNP@α-CD-*E*-azo/XLG. The absorption peak at about 480 nm demonstrated that the drug DOX were successfully loaded into the hydrogel (**Fig. S19**). The drug encapsulation rate was calculated as ~95%. The drug release was first evaluated in the dark at 37 °C (**Fig. 3a**): the release was pH sensitive and favored an acidic environment (34.6±1.1% at pH 5.0 *vs*. 1.6±0.8% at pH 7.4). Then we monitored DOX releasing at pH 5.0 in the dark for 60 min followed by NIR irradiation (**Fig. 3b**), showing that the NIR light can evidently boost the release even at low pH. The DOX release followed an irradiation-duration dependent fashion (**Fig. 3c**): under 980 nm irradiation (1 W cm^{-2}), it took 30 min to release 38.9±2.0% and 4 h to release 61.7±1.9%. The influence of irradiation intensity was also explored: upon 4h irradiation, the total release was enhanced from 61.7±1.9% to 88.7±2.1% when the applied irradiation density increased from 1 W cm^{-2} to 3 W cm^{-2}. Moreover, a distinct "on-off" pattern of the release was observed when the NIR light was switched on then off in the dark at pH 5.0 (**Fig. S20**), suggesting the possibility of remotely controlling the release process and release dose by varying NIR intensity.

Photothermal effect of the SHGs. In addition, the UCNPs have a good photothermal effect,[20] thus we investigated the effect of temperature on the SHGs. Upon NIR light irradiation, the temperatures of UCNP@α-CD and UCNP@α-CD-*E*-azo/XLG increased linearly when increasing power density in a range of 0–3.0 W cm^{-2}, while the pure XLG had little change (**Fig. 3d**). The excellent photothermal properties of the SHGs were proved, the temperature increased about 8.0 °C with 980 nm light irradiation. Then, the effect of temperature on the hydrogel phase transition was studied. When heated to 45.0 °C externally, pure XLG had a phase transition, but DOX-loaed SHGs still remain hydrogel state (**Fig. S21**). The drug release behavior of pure XLG and DOX-UCNP@α-CD-*E*-azo/XLG were presented in **Fig. S22** and **Fig. 3a**. DOX release in DOX-UCNP@α-CD-*E*-azo/XLG did not change significantly at 37.0 °C and 45.0 °C. These results suggested that NIR irradiation of the SHGs can produce photothermal effects, but the resulting heat cannot cause a phase transition. The phase transition occured only in the condition of NIR irradiation.

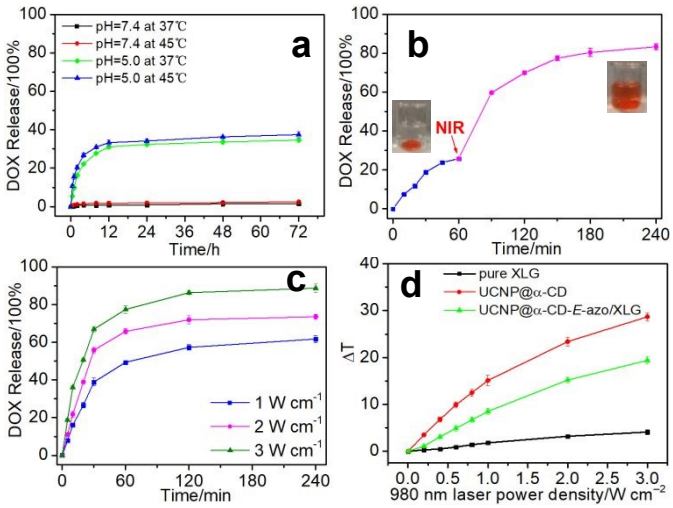

Fig. 3 DOX release from the DOX-UCNP@α-CD-*E*-azo/XLG hydrogel (a) in pH 7.4 and pH 5.0 at different temperature under the dark, respectively, (b) at pH 5.0 when keeping in the dark for first 60 min and irradiated by NIR light afterwards (Inset: photographs of the SHG, showing the obvious change of the red zone before and after drug release), (c) at pH 5.0 upon NIR irradiation of various power density. The NIR irradiation is 980 nm (1 W cm^{-2}). (d) The temperature changes of pure XLG, UCNP@α-CD, UCNP@α-CD-*E*-azo/XLG in aqueous dispersion under NIR light irradiation at various power densities. Samples were dispersed in aqueous solution at the same concentration.

In *Vitro* Cell Cytotoxicity and NIR-Responsive Treatment. To explore the celluar uptake performance of the SHGs, HepG2 cells were incubated with DOX-UCNP@α-CD-*E*-azo/XLG for 1.0 and 3.0 h in the dark as well as 3.0 h under NIR irradiation, respectively, then stained with 4',6-diamidino-2-phenylindole (DAPI). From **Fig. 4**, different from the control group where no red signal was observed, red fluorescence corresponding to DOX was presented in the cells after 1 h incubation with the SHG in the dark, implying the effective cellular uptake of the SHG. The red signal was enhanced when the incubating period was extended from 1.0 h to 3.0 h. Importantly, by combination of the SHG with NIR irradiation, the red fluoresence was largely boosted, and the signal distribution varied from cytoplasm to nuclei as well. The results indicate that NIR irradiation can not only enhance the celluar uptake of the SHG, but also trigger the drug release.

The therapeutic performance of the SHGs was first examined *in vitro* on HepG2 (a cancer cell line) and L02 cells (a normal cell line) by MTT assay. When incubating with UCNP@α-CD-*E*-azo/XLG and DOX-UCNP@α-CD-*E*-azo/XLG at a concentration up to 1000 μg mL^{-1} in the dark for 24 h, respectively, the cell viability of both cells was barely reduced (**Fig. S23a and S24a**), indicating the stability and low cytotoxicity of the SHG if any. Interestingly, upon NIR illumination (980 nm, 1 W cm^{-2}, 30 min), UCNP@α-CD-*E*-azo/XLG (250 μg mL^{-1}) without loading the drug can already induce cell death of ~24.7% to the treated HepG2 (**Fig. S23b**). The photothermal effect of UCNPs causes a rise in temperature, which could kill some cancer cells.

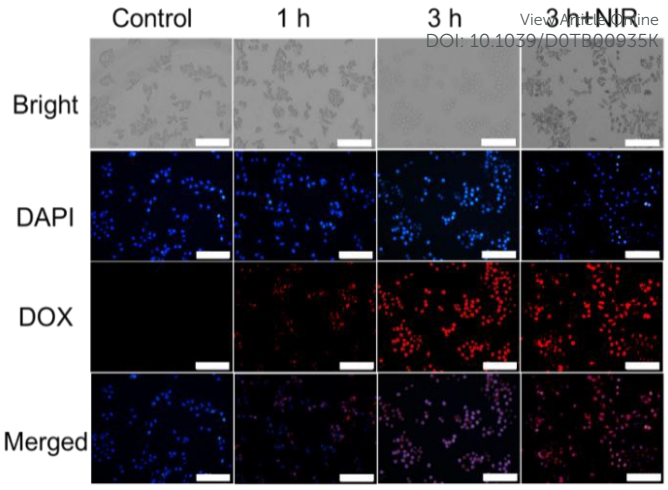

Fig. 4 Bright optical images and fluorescence images of HepG2 cells treated without (Control), with DOX-UCNP@α-CD-*E*-azo/XLG (250 μg mL^{-1}) for 1 and 3h in the dark (1h and 3h), and with DOX-UCNP@α-CD-*E*-azo/XLG (250 μg mL^{-1}) with 980 nm light irradiation for 30 min at 1 W cm^{-2} (3h + NIR). The cells were stained with DAPI after various treatments. Based on the merged images of DAPI (blue) and DOX signal (red), the distribution of DOX in the cell can be revealed. The NIR irradiation is 980 nm (1 W cm^{-2}) for 30 min, Scale bar = 50 μm.

Since the UCNPs and the polymer in the UCNP@α-CD-*E*-azo/XLG are known for high biocompatibility, the results thus imply that the gel-to-sol phase transition UCNP@α-CD-*E*-azo/XLG upon NIR irradiation has certain effect on cancer cell inhibition. Reasonably, the inhibition effect was largely improved with the released drug: for HepG2 cells incubated with DOX-UCNP@α-CD-*E*-azo/XLG at the same concentration, the cell viability decreased to 31.4±3.5 %, due to the efficient drug release upon the NIR irradiation (**Fig. S23b**). Notably, after the same combined treatment, the survival rate of normal cells L02 (58.5±2.66 %) are higher than that of cancer cells (**Fig. S24b**). It revealed the toxicity specificity of the SHGs on cancer cells. That is because the acidic environment around cancer cells promotes drug release, in consistent with previous literatures.[21] To intuitively demonstrate the cancer cell inhibition effect of the SHG *in vitro*, the DOX-UCNP@α-CD-*E*-azo/XLG (250 μg mL^{-1}) treated HepG2 cells were stained with propidium iodide (PI), and red fluorescent signals were used to distinguish dead cells.

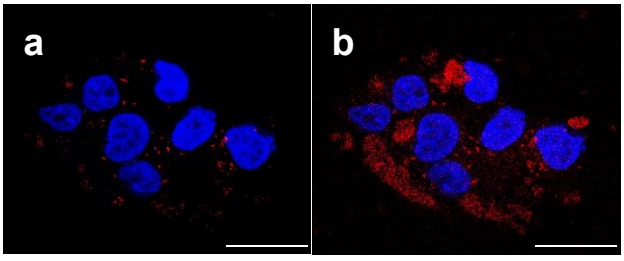

Fig. 5 CLSM images of DOX-UCNP@α-CD-*E*-azo/XLG hydrogel in HepG2 cells before (a) and after (b) NIR light irradiation for 30 min (980 nm, 1 W cm^{-2}). Scale bar = 25 μm.

As shown in **Fig. S25b-j**, the cells in the control group presented no significant red signal, revealing the low toxicity of the SHG. In consistent with the results of MTT assay, applying combination of 250 μg mL^{-1} DOX-loaded SHGs with NIR light (980 nm, 1 W cm^{-2}) illuminate for 30 min which killed the cancer cells effectively, illustrated by the apparently increased red signal in the fluorescence image (**Fig. S25l**). Besides, the internalization process was monitored to determine intracellular localization and distribution (**Fig. 5**). From the CLSM (confocal laser scanning microscopy) pictures, a relatively little amount of bright red fluorescent spots were observed. However, strongerred fluorescence appeared in the cytoplasm after NIR irradiation. The result confirmed that the SHG are stable enough in a complex cellular environment before NIR irradiation. And when the azobenzene was photoisomerized, the loaded SHG went through a gel-to-sol phase conversion led to more drugs release.

In *Vivo* NIR-Responsive Treatment. Motivated by the above-described *in vitro* anticancer effect, the phototherapeutic efficacy of the SHGs *in vivo* was studied further. HepG2 tumor-bearing nude mice subcutaneously as a tumor model, and all mice were divided into six groups (five mice in each group) at random for different experimental conditions: PBS injection only (Group 1), NIR irradiation only (Group 2), UCNP@α-CD-*E*-azo/XLG injection only (Group 3), UCNP@α-CD-*E*-azo/XLG injection plus NIR irradiation (Group 4), DOX-UCNP@α-CD-*E*-azo/XLG injection only (Group 5), and DOX-UCNP@α-CD-*E*-azo/XLG injection plus NIR irradiation (Group 6) (**Fig. S26a**).

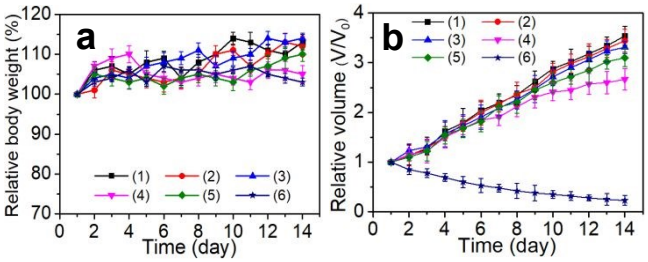

Fig. 6 (a) Relative body weights and (b) relative tumor volumes of the mice in groups 1–6. All mice were divided into six groups: PBS injection only (Group 1), NIR irradiation only (Group 2), UCNP@α-CD-*E*-azo/XLG injection only (Group 3), UCNP@α-CD-*E*-azo/XLG injection plus NIR irradiation (Group 4), DOX-UCNP@α-CD-*E*-azo/XLG injection only (Group 5), and DOX-UCNP@α-CD-*E*-azo/XLG injection plus NIR irradiation (Group 6). The NIR irradiation is 980 nm (1 W cm^{-2}) for 30 min.

As shown in **Fig. 6a**, during the experiment period of 14 days, the weight changes of all mice in the control and treatment groups were negligible, indicating that these treatments had less adverse effects. Tumor volumes in six groups were surveyed and mapped with time (**Fig. 6b**). In consistent with the *in vitro* results, whilst the tumors in Group 1-5 showed similar pattern that was no much different. Remarkbly the inhibition rate of DOX-UCNP@α-CD-*E*-azo/XLG injection plus NIR irradiation (Group 6) was as as 0.23±1.27 % after 14 days. Among all the groups, the tumor of Group 6 was the smallest (**Fig. S26b**). Moreover, the tumor tissue sections with hematoxylin and eosin (H&E) staining (**Fig. S26c**) revealed the most severe tissue damage from Group 6. All these results emphasize the high antitumor competency of the drug-loaded SHG under NIR irradiation, which are attributed to the NIR-driven gel-to-sol phase transition hence the efficient drug release, and release of UCNP@α-CD simultaneously which can generate photothermal therapy. Therefore, the the synergy of chemotherapy and photothermal treatment is achieved.

We eventually researched the toxicity of the drug-loaded SHG *in vivo*. After staining with H&E in groups 1–6 of all mice, there were no evident abnormalities or biological damage to the heart, liver, spleen, lung, and kidney at 14th day, demonstrating low/no systemic toxicity of SHGs injection on the major organs of mice (**Fig. 7**). We also carried out hematological analysis of white blood cell (WBC), red blood cell (RBC), mean corpuscular volume (MCV), hematocrit (HCT), hemoglobin (HGB), mean corpuscular hemoglobin (MCH), mean corpuscular hemoglobin concentration (MCHC), platelet (PLT), mean platelets volume (MPV) and plateletcrit (PCT) on 14th day after treatment, respectively. Encouragingly, these measures were within the normal range (**Fig. S27**). The combination of these results confirmed that the SHG with/without drug loading possess good biocompatibility.

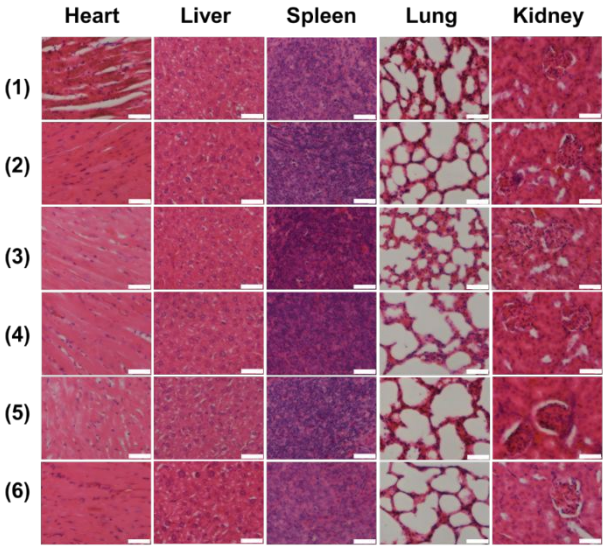

Fig. 7 Histology staining of major organs (heart, liver, spleen, lung, and kidney) dissected from various treatments groups at 14th day. All mice were arbitrarily divided into six groups: PBS injection only (Group 1), NIR irradiation only (Group 2), UCNP@α-CD-*E*-azo/XLG injection only (Group 3), UCNP@α-CD-*E*-azo/XLG injection plus NIR irradiation (Group 4), DOX-UCNP@α-CD-*E*-azo/XLG injection only (Group 5), and DOX-UCNP@α-CD-*E*-azo/XLG injection plus NIR irradiation (Group 6). The NIR irradiation is 980 nm (1 W cm^{-2}) for 30 min, scale bar = 50 μm.

Conclusions

In conclusion, our work presents synthesis method and application prospect of UCNP@α-CD-*E*-azo/XLG SHGs featuring reversible gel-to-sol phase transition driven by NIR irradiation, as a release-controllable drug carrier for cancer treatment. When the SHG was irradiated with NIR light, the UV light emitted by UCNP caused the structure isomerization of azobenzene, resulting in the escape from the cyclodextrin cavity. The SHG showed low/no cytotoxicity and stability to prevent early leakage. By injection to the tumor site directly and then exposure to NIR light, the hydrogels can release drug effectively and produce local heat by photothermal conversion. Both *in vitro* and *vivo* experiments have proven its effective inhibitory effect on tumors. By changing the dose or duration of NIR exposure, the controllable amount of drug release can be achieved. Considering the excellent drug loading and retaining rate as well as the remotely controllable NIR-responsiveness and remarkable chemotherapy and photothermal output and efficacy, this work provides an exciting new candidate for antitumor therapy and other site-specific treatments such as dental or medical implant associated infections, especially those requiring long-term, small-dose treatments in clinic.

Conflicts of interest

There are no conflicts to declare.

Acknowledgements

We thank NNSFC (91860120) for financial support.

References

1 (a) Y. M. Zhang, N. Y. Zhang, K. Xiao, Q. Yu, Y. Liu, *Angew. Chem. Int. Ed.,* 2018, **57**, 8649; (b) Q. Yu, Y.-M. Zhang, Y.-H. Liu, X. Xu, Y. Liu, *Sci. Adv.,* 2018, **4**, 2297; (c) P. Xing, Y. Zhao, *Small Methods,* 2018, **2**, 1700364; (d) L. Zhao, Y. Liu, R. Chang, R. Xing, X. Yan, *Adv. Funct. Mater.,* 2019, **29**, 1806877.

2 (a) M. J. Webber, E. A. Appel, E. W. Meijer, R. Langer, *Nat. Mater.,* 2015, **15**, 13; (b) X. Du, J. Zhou, J. Shi, B. Xu, *Chem. Rev.,* 2015, **115**, 13165.

3 M. J. Webber, R. Langer, *Chem. Soc. Rev.,* 2017, **46**, 6600.

4 (a) A. G. Cheetham, P. Zhang, Y. A. Lin, L. L. Lock, H. Cui, *J. Am. Chem. Soc.*, 2013, **135**, 2907-2910; (b) X. Ma, Y. Zhao, *Chem. Rev.*, 2015, **115**, 7794-7839; (c) K. Ulbrich, K. Holá, V. Šubr, A. Bakandritsos, J. Tuček, R. Zbořil, *Chem. Rev.,* 2016, **116**, 5338-5431.

5 (a) X. Du, J. Zhou, J. F. Shi, B. Xu, *Chem. Rev.*,2015, **115**, 13165; (b) J. Li, D. J. Mooney, *Nat. Rev. Mater.*, 2016, **1**, 16071; (c) S. Naahidi, M. Jafaric, M. Logana, Y. Wang, Y. Yuan, H. Bae, B. Dixon, P. Chen, *Biotechnol. Adv*., 2017, **35**, 530; (d) J. Y. C. Lim, S. S. Goh, S. S. Liow, K. Xue, X. J. Loh, *J. Mater. Chem. A.*, 2019, **7**, 18759; (e) B. O. Okesola, D. K. Smith, *Chem. Soc. Rev.*, 2016, **45**, 4226; (f) Y. Hu, Z. Wang, D. Jin, C. Zhang, R. Sun, Z. Li, K. Hu, J. Ni, Z. Cai, D. Pan, X. Wang, W. Zhu, J. Li, D. Wu, L. Zhang, J. Chu, *Adv. Funct. Mater.,* 2020, **30**, 2070026.

6 (a) L. A. Wilkinson, K. B. Vincent, A. J. H. M. Meijer, N. J. Patmore, *Chem. Commun.*, 2016, **52**, 100; (b) A. Rey-Rico, M. Cucchiarini, *Polymers*, 2019, 11, 514; (c) M. R. Saboktakin, R. M. Tabatabaei, *Int. J. Biol. Macromol.*, 2015, **75**, 426; (D) L. Wang, X. Shi, J. Zhang, Y. Zhu, J. Wang, *RSC Adv.*, 2018, **8**, 31581.

7 (a) C. Wang, J. Wang, X. Zhang, S. Yu, D. Wen, Q. Hu, Y. Ye, H. Bomba, X. Hu, Z. Liu, G. Dotti, Z. Gu, *Sci. Transl. Med*., 2018, **10**, 3682; (b) Q. Chen, C. Wang, X. Zhang, G. Chen, Q. Hu, H. Li, J. Wang, D. Wen, Y. Zhang, Y. Lu, G. Yang, C. Jiang, J. Wang, G. Dotti, Z. Gu, *Nat. Nanotechnol*., 2019, **14**, 89; (c) J. Li, D. J. Mooney, *Nat. Rev. Mater*., 2016, **1**, 16071.

8 (a) W. Bensaïd, J. T. Triffitt, C. Blanchat, K. Oudina, L. Sedel, H. Petite, *Biomaterials,* 2003, **24**, 2497; (b) L. Yu, J. Ding, *Chem. Soc. Rev.*, 2008, **37**, 1473; c) F. Wang, Z. Li, M. Khan, K. Tamama, P. Kuppusamy, W. R. Wagner, C. K. Sen, J. Guan, *Acta Biomater.*, 2010, **6**, 1978.

9 (a) X. Yu, K. Yang, X. Chen, W. Li, *Biomaterials*, 2017, **143**, 120; (b) W. Huang, Y. Huang, Y. You, T. Nie, T. Chen, *Adv. Funct. Mater.*, 2017, **27**, 1701388; (c) W. Tao, X. Ji, X. Xu, M. A. Islam, Z. Li, S. Chen, P. E. Saw, H. Zhang, Z. Bharwani, Z. Guo, J. Shi, O. C. Farokhzad, *Angew. Chem. Int. Ed.*, 2017, **56**, 11896.

10 (a) X. Wang, C. Wang, Q. Zhang, Y. Cheng, *Chem. Commun*., 2016, **52**, 978; (b) A. Vashist, A. Kaushik, K. Alexis, R. Dev Jayant, V. Sagar,A. Vashist,M. Nair, *Curr Pharm Des.*, 2017, **23**, 3595.

11 A. Harada, M. Furue, S.-i. Nozakura, *Polym. J.,* 1980, **12,** 29.

12 G. Yu, C. Han, Z. Zhang, J. Chen, X. Yan, B. Zheng, S. Liu, F. Huang, *J. Am. Chem. Soc*., 2012, **134**, 8711.

13 T. Zhang, H. Lin, L. Cui, N. An, R. Tong, Y. Chen, C. Yang, X. Li, F. Qu, *RSC Adv.* 2016, **6**, 26479-26489.

14 (a) C. Ma, T. Bian, S. Yang, C. Liu, T. Zhang, J. Yang, Y. Li, J. Li, R. Yang, W. Tan, *Anal. Chem*., 2014, **86**, 6508; (b) J. C. Boyer, C. J. Carling, S. Y. Chua, D. Wilson, B. Johnsen, D. Baillie, N. R. Branda, *Chem. Eur. J*., 2012, **18**, 3122.

15 D. Zhao, Y. Chen, Y. Liu, *Chem. Eur. J*., 2014, **9**, 1895.

16 (a) H. S. Qian, Y. Zhang, *Langmuir,* 2008, **24**, 12123; (b) R. Abdul Jalil, Y. Zhang, *Biomaterials,* 2008, **29**, 4122; (c) N. M. Idris, Z. Li, L. Ye, E. K. Wei Sim, R. Mahendran, P. C.-L. Ho, Y. Zhang, *Biomaterials,* 2009, **30**, 5104.

17 Z. Q. Li, Y. M. Zhang, H.-Z. Chen, J. Zhao, Y. Liu, *J. Org. Chem.,* 2013, **78**, 5110.

18 L. Fang, T. Fang, X. Liu, Y. Ni, C. Lu, Z. Xu, *Compos. Sci. Technol.,* 2017, **152**, 190.

19 (a) Z. Q. Li, Z. H. Hou, H. X. Fan, H. R. Li, *Adv. Funct. Mater.*, 2017, **27**, 1604379; (b) Z. Q. Li, G. N. Wang, Y. G. Wang, H. R. Li, *Angew.Chem. Int. Ed.,* 2018, **57**, 2194.

20 M. Gonçalves, P. Figueira, D. Maciel, J. Rodrigues, X. Qu, C. Liu, H. Tomás, Y. Li, *Acta. Biomater.,* 2014, **10**, 300.

21 Y. Wu, R. Guo, S. Wen, M. Shen, M. Zhu, J. Wang, X. Shi, *J. Mater. Chem. B*, 2014, **2**, 7410.

View Article Online
DOI: 10.1039/D0TB00935K

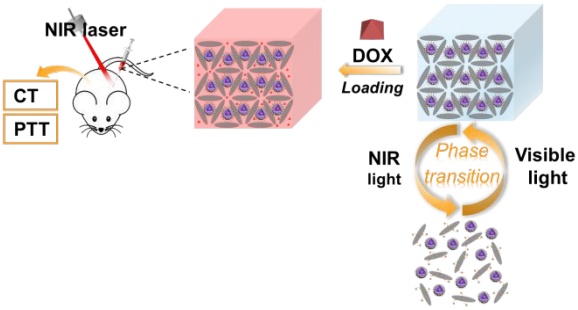

We report injectable supramolecular hydrogels as high-load drug carriers, which achieve the synergy of chemotherapy and photothermal treatment for cancer.